PHILOSOPHICAL TRANSACTIONS OF THE ROYAL SOCIETY A MATHEMATICAL, PHYSICAL & ENGINEERING SCIENCES

Geophysical Evidence for the Role of Fluids in Accretionary Wedge Tectonics

G. K. Westbrook

Phil. Trans. R. Soc. Lond. A 1991 **335**, 227-242
doi: 10.1098/rsta.1991.0044

Geophysical evidence for the role of fluids in accretionary wedge tectonics

By G. K. Westbrook

School of Earth Sciences, University of Birmingham, Edgbaston, Birmingham B15 2TT, U.K.

The seismic-reflection technique, by imaging lithological and structural boundaries, can largely define the framework upon which models of the fluid-flow régimes of accretionary wedges are hung. The distribution of fluid loss from the sediments that form the accretionary wedge and that lie beneath it, can be estimated from variation in seismic velocity as a measure of change in porosity, in conjunction with the interpretation of the structural evolution derived from seismic-reflection sections. Seismic techniques have detected regions of pronounced undercompaction believed to be associated with overpressured pore fluid, and detailed modelling has defined zones of localized fluid overpressuring, such as the decollements beneath wedges. The measurement of heat flow, directly, or indirectly from the methane-hydrate seismic reflector, can be used to detect the outflow of fluids, and map its variation in relation to structure and lithology. Geophysical techniques will achieve their full potential in constraining models of the behaviour of accretionary wedges, when calibrated from borehole measurements.

1. Seismic techniques

Seismic techniques have provided the principal means of determining the structure and physical properties of accretionary wedges. It is doubtful whether most of the current concepts of processes in accretionary wedges would have been developed if it had not been for the seismic reflection sections across convergent plate margins. Certainly, seismic reflection sections show to a greater or lesser degree, the internal architecture of an accretionary wedge and can provide information on changes in physical properties that are related to its fluid-flow régime. Although seismic reflection images are sometimes very limited in what they show of the internal structure of accretionary wedges, there is no comparable technique to define the configuration of the structures and beds from which may be inferred the distribution of permeability and the mechanisms of deformation that generate the excess pore fluid pressure that drives fluid flow. To define the hydrogeological system of an accretionary wedge, measurements of the hydrogeological properties of samples and *in situ* tests of fluid pressure and permeability from boreholes with measurements of fluid outflow at the surface, are needed to complement the structural information obtained from seismic reflection. Even without this important calibration, however, seismic reflection can be used as a guide to major elements of the fluid-flow régime (figure 1). The position of the decollement horizon in the sedimentary section can strongly influence where porewater is expelled from the sediment by compaction. If

Phil. Trans. R. Soc. Lond. A (1991) **335**, 227–242
Printed in Great Britain

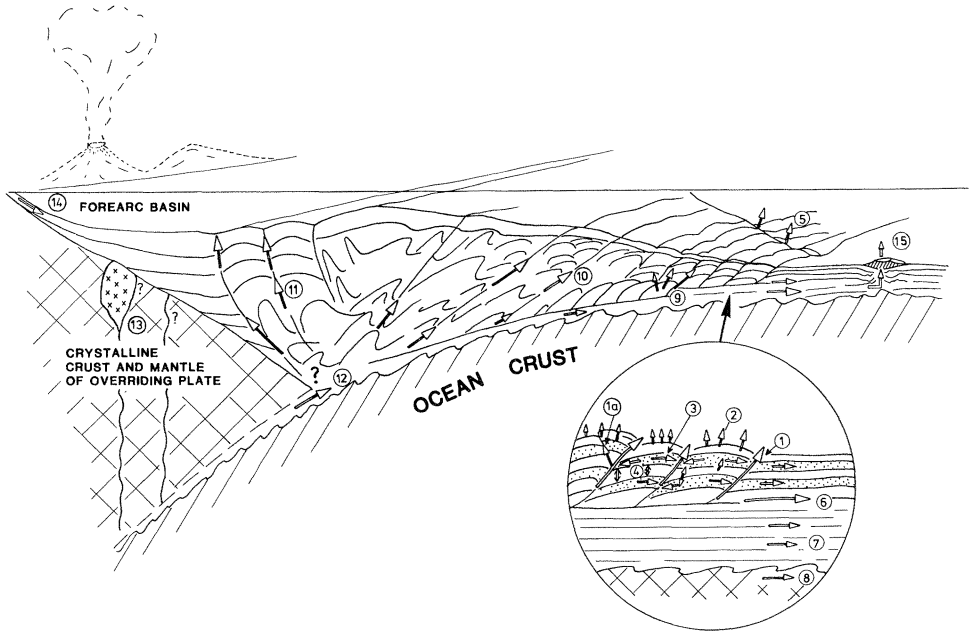

Figure 1. Illustration of modes of fluid outflow from an accretionary wedge (after Westbrook *et al.* 1987). (1) Fluid escape along thrust fault associated with accretion at the front of the wedge, and (1a) along faults antithetic to these. (2) Diffuse flow out of the sea bed in response to compaction. Fractures produced by local tensile stress at crests of anticlines may aid outflow. (3) Lateral flow along more permeable units in accreted sequence, feeding flow to faults. (4) Flow from less permeable units into more permeable units. (5) Outflow from vertical strike–slip faults intersecting the accretionary wedge. (6) Horizontal flow along the decollement beneath the wedge. (7) Outward flow in sequence beneath wedge in response to the load of the wedge. (8) Flow in permeable upper part of oceanic igneous crust. (9) Release of water into the wedge as a consequence of the deformation of subcreted (underplated) packets of sediment in duplexes. (10) Flow along major out-of-sequence landward dipping, thrusts that enable the wedge to maintain its critical taper. Local dilation and vein deposits from outflowing water may be the cause of acoustic impedance contrasts that gives these faults seismic visibility. (11) Flow along backthrusts into the forearc basin. (12) Upflow from deeper parts of the subduction zone of water released by dehydration reactions. This will be dependent to some degree on subduction rate. (13) Water from deeper part of subduction zone penetrating fractures in overriding lithosphere. Fractures are probably radial to the island arc. Hydration of the ultramafic rock may cause formation of serpentinite diapirs. (14) Meteoric groundwater from island arc or cordilleran continental margin seeping into horizons in the forearc basin, and then out into basin. (15) Outflow through mud volcano on ocean floor in front of wedge.

the decollement is deep and most of the section becomes accreted to the toe of the wedge then much of the fluid will be released near the toe (Davis *et al.* 1990). A shallow decollement above a thick section of sediment introduces the possibility of a larger proportion of the fluids in the sedimentary section being underthrust farther beneath the wedge (Westbrook *et al.* 1988), to be released into the wedge above, to flow back oceanward into the undeformed section along the higher permeability units in the underthrust sequence or the decollement (Westbrook & Smith 1983; Moore *et al.* 1988), or to be carried down into the mantle. Off Costa Rica, the landward convergence of reflectors in the underthrust sequence of hemipelagic and pelagic sediments beneath the outermost 4 km of the wedge indicates rapid compaction and water loss (Shipley & Moore 1986; Shipley *et al.* 1990). If the original

thickness of the layer and the relationship between seismic velocity and porosity are known, the amount of compaction and fluid loss can be calculated, which for the Costa Rica example is 0.0025 $m^3\ m^{-2}\ a^{-1}$ over the surface area of the underthrust section. Expressed differently, the hemipelagic and pelagic layers lose 44 % and 58 % of their original content of water by the time they have moved a horizontal distance of 4 km beneath the toe of the wedge at a rate of 90 km Ma^{-1}. At the toe of the northern part of the Barbados accretionary wedge, the compaction undergone by the underthrust section is slight, and difficult to measure accurately on the seismic sections (Bangs *et al.* 1990). Measurements of the porosity of samples obtained from drilling there show that only 4 % of the original volume of pore fluid is lost in the first 4 km of underthrust section (Moore *et al.* 1988). This approach to estimating compaction depends strongly on knowing the original thickness of the layer or assuming that it was the same as that in the undeformed section in front of the wedge. This assumption may often not be justified, particularly if the underthrust section includes part of the turbidite fill of the trench.

2. Seismic velocity

Variation in seismic velocity has been used widely to estimate changes in porosity caused by compaction of sediments in accretionary wedges. These changes in porosity may be used to derive, with decreasing certainty, fluid outflow and fluid pressure. The techniques used to measure seismic velocity, fall mostly into two categories: (*a*) velocity analysis of precritical reflections from multichannel seismic lines run across the strike of the structures in a wedge, (*b*) analysis of the pre- and post-critical reflections and refracted phases from lines run parallel to the strike. Velocity analyses from multichannel seismic surveys have been used to estimate porosity by Bray & Karig (1985), Minshull & White (1989), Davis *et al.* (1990), and Bangs *et al.* (1990), but only in the work reported by Bangs *et al.* for the Barbados Ridge accretionary wedge, was the aperture of the seismic experiment (5 km) designed with velocity derivation as a specific objective and a method of analysis employed to minimize the statistical and deterministic errors in the data (every common midpoint gather was used for velocity analysis and velocities were corrected for dip). The analyses of data from wide-angle reflection and refraction experiments shot along strike usually provide more precisely determined functions of velocity with depth than those obtained from precritical reflections, but these velocity/depth functions can be quite inaccurate. This is because the techniques commonly used, expanding spread seismic profiles (ESPS) and unreversed lines shot to sonobuoys, have no inherent control on the effect of dip on velocity (ESPS are better than simple unreversed lines), and so depend on remaining perfectly parallel to strike unless seismic reflection lines show the dips of major seismic boundaries. The advantages of these techniques are that they can yield accurate velocities to greater depths in the wedge, the inversion of the travel time data to velocity/depth is simpler because the problems of lateral variation of the velocity field are avoided, and, perhaps most importantly, the refracted phases can yield the velocity structure in regions where there are no distinct reflectors. The disadvantages are that the techniques cannot be used to map the variation in velocity continuously across the wedge, and cannot be used to examine porosity variation within individual structures. If refracted phases alone are used, reversals of velocity with depth can cause problems for inversion schemes. Commonly, such as in the Barbados Ridge accretionary complex, the

PHILOSOPHICAL TRANSACTIONS OF THE ROYAL SOCIETY A MATHEMATICAL, PHYSICAL & ENGINEERING SCIENCES

analyses of data from ESPs and sonobuoys, generally show higher velocities than those from the multichannel reflection data. The wider offset ESPs and sonobuoys, have a much greater horizontal component in their ray paths, and where there are closely spaced, layers of high and lower velocity, the average horizontal velocity is biased towards the higher velocities (in fact inversion of the refraction data usually only determines the horizontal velocity). The most generally useful type of velocity data for investigating accretionary wedges is that which comes from a multichannel reflection survey, provided that it has sufficient aperture, and provided that there are sufficient seismic reflectors. The velocity analyses, however, need to be much more extensive than those usually conducted to produce a seismic reflection section. They should be on data which has been corrected for dip moveout, and ray tracing and velocity determination coupled to migration may be required, especially if large lateral velocity contrasts occur within an accretionary wedge.

Velocity data from accretionary wedges, even though they vary in type and quality, have already provided important information on the response of sediments to being accreted and to being underthrust. Porosity has been derived from velocity through empirically based relationships such as that of Hamilton (1978) for silt, mudstone and turbidite lithologies. This is not an accurate method of determining absolute values of porosity, but it is adequate for showing changes in porosity in formations of predominantly the same lithology. Data from wedges that have accreted turbidites with a high sand fraction, such as off the Makran (Fowler *et al.* 1985; Minshull & White 1989) and off Vancouver (Davis *et al.* 1990), indicate that water is lost rapidly from the accreted section near the toe of the wedge, and that the sedimentary section is overcompacted relative to undeformed section in the trench. Off Barbados, in the north where the accreted section is predominantly pelagic clays, the porosity/depth profile in the first 20 km of the wedge is one of undercompaction, even though all the accreted sediments have undergone some compaction relative to their pre-accreted state (Bangs *et al.* 1990; Taylor & Leonard 1990). The reason for this effect is that sediments buried more deeply by tectonic thickening have not responded fully in reducing their porosities to those normally appropriate for their depths, because low permeability has inhibited the release of porewater. Farther south, where the accreted section is predominantly composed of distal turbidites it shows no significant change in the porosity/depth profile in the first 20 km, even though it increases in thickness by 1.1 km (a proportional increase of 1.6). To understand the history of compaction and dewatering of the sediment, the mechanics of thickening of the wedge must be known. This is illustrated with an example from the Barbados Ridge accretionary complex (figure 2). Line 480 crosses the wedge at 14° 22′ N (Bangs *et al.* 1990; Ladd *et al.* 1990), where a 1.9 km thick section of distal turbidites in the Orinoco submarine fan is being accreted above a 1.4 km thick section of predominantly pelagic and hemipelagic sediments. The section has been thickened primarily by thrusting along faults that dip at 30° through most of the section, but which curve toward horizontal in the upper part of the section where the least consolidated part of the section is overridden. Porosity in the section was derived from seismic velocity (Bangs *et al.* 1990). The pre-accretion porosity/depth profile, derived from the section in front of the wedge (after a small correction for the westward stratigraphic thickening of the section before accretion), was then subtracted from each thrust slice, following the internal stratigraphy, to map the change in porosity. The proportional changes in volume were calculated from $((\phi_0-\phi_1)/(1-\phi_1))$, where ϕ_0 is the initial porosity and ϕ_1 is the final porosity. The

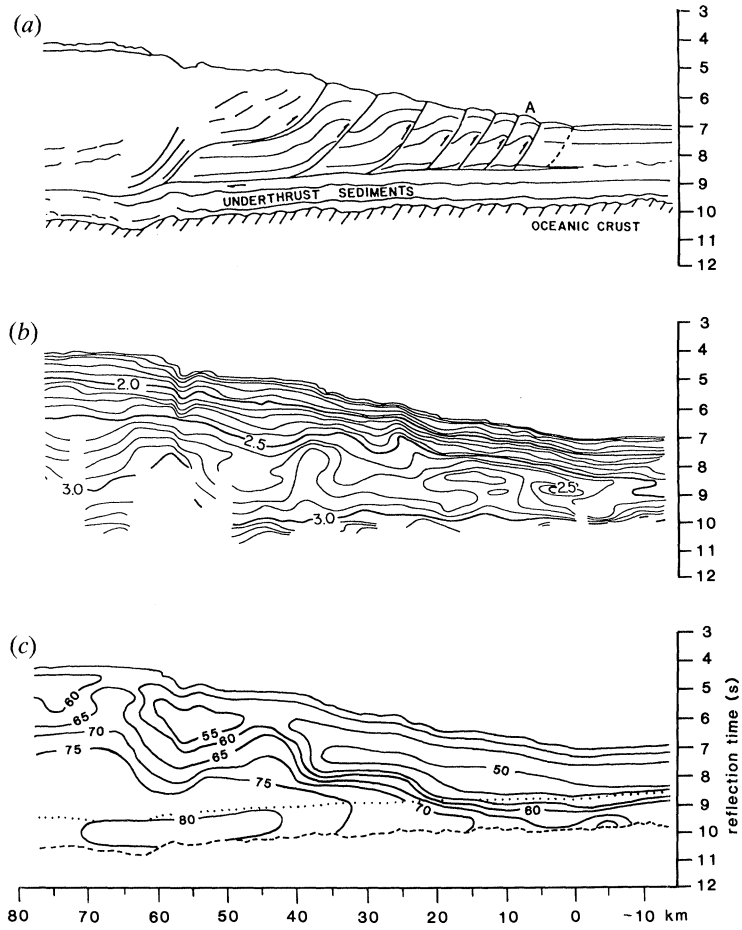

Figure 2. Illustration of the relationship between structure and fluid pressure inferred from seismic velocity, at the front of the Barbados Ridge accretionary complex, seismic line 480, 14° 22′ N. (*a*) Line drawing of major reflectors and interpretation of structure. (*b*) Contours of P-wave, seismic velocity, at 0.1 km s^{-1} intervals. (*c*) Contours of λ (ratio of fluid pressure to lithostatic pressure) expressed as percentages. Fluid pressures are derived through the assumption that velocity reflects the effective stress in a reference sedimentary section in which fluid is at hydrostatic pressure throughout. Dotted line shows the position of the decollement. Dashed line shows the position of the oceanic igneous basement.

resulting section of volume loss (illustrated for one thrust slice in figure 3) shows no loss from the axial regions of the uplifted anticlines, and maximum volume loss in the footwall sections of the thrusts especially in the upper, and initially least consolidated parts where it can be as much as 30%. Simple models of accretion used to model fluid flow (Screaton *et al.* 1990) and heat flow (Langseth *et al.* 1990), or both (Le Pichon *et al.* 1990) are often ones in which the accreted sediment flows into a fixed wedge taper, slowing as its streamlines diverge to follow the sides of the wedge. In these models the sediment is usually assumed to have an exponential porosity/depth function and as it thickens in the wedge, each unit of sediment increases its depth beneath the wedge surface and becomes more compacted, releasing fluid. The maximum rate of fluid loss occurs about 1 km beneath the surface, because the rate of change depth with increasing horizontal distance into the wedge increases with

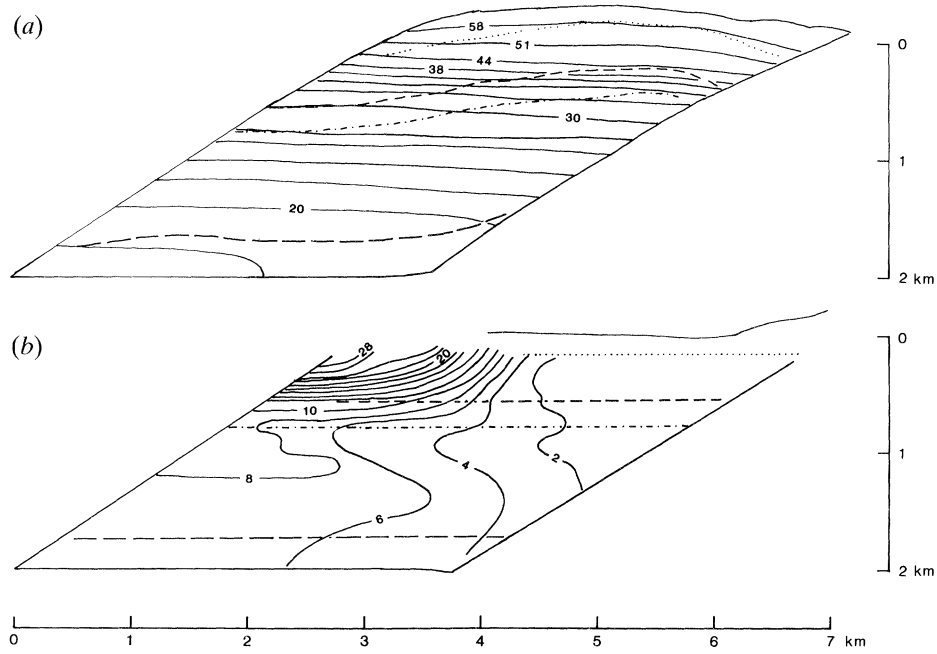

Figure 3. Porosity variation in and fluid loss from a thrust slice at the toe of the Barbados Ridge accretionary wedge imaged on seismic line 480, marked A in figure 2. (*a*) Shape of thrust slice with contours of porosity expressed as percentages, derived from seismic velocity. Major seismic reflectors marked by dashed and dotted lines. (*b*) Thrust slice restored to shape before deformation, with contours of percentage volume decrease from original volume.

depth, whereas porosity decreases with depth. This is not the same distribution of fluid loss as that derived from the porosity data from seismic velocity (figure 3). The important difference of the model is that it has no mechanism for strongly loading the near-surface section. The data and the model show about the same overall loss of fluid, but the difference in distribution is significant. Fluids derived from deeper in the section will have a much greater effect on heat flow and their pore-fluid chemistry could be significantly different, depending on thermally dependent reactions and variation in lithology with depth.

Pore fluid pressures may be estimated from the differences between actual porosity and porosity in a normal sedimentary section at the same depth, given two important assumptions. These assumptions are that sediments are steadily compacting (i.e. water is leaving the pore spaces under a load which has always been increasing) and that the reference (expected) porosity represents that developed at hydrostatic pressure. Porosity and effective stress (difference between lithostatic pressure and hydrostatic pressure) can be related through the compressibility of the sediment, as Shi & Wang (1988) have done in their modelling of pore fluid pressures in accretionary wedges, but compressibility in clays changes with degree of consolidation and effective stress and does not take the same value during unloading that it has during loading (Taylor & Leonard 1990). To avoid this complication, porosity was related to effective stress through the reference porosity/depth curve (Bangs *et al.* 1990), assuming that the water was at hydrostatic pressure throughout, that its density was 1050 kg m^{-3} and the sediment grain density was 2700 kg m^{-3}. As the porosity/velocity relationship is defined (Hamilton 1978), the effective stress can

be directly related to velocity, so contours of effective stress follow those of velocity. Using velocity to indicate effective stress, and calculating lithostatic stress by integrating the density of the overlying sediments over their thickness, the ratio of fluid pressure to lithostatic pressure (λ) can be calculated. This was carried out on seismic data from the Barbados Ridge Complex, and shows that values of λ just reach 0.8 in the underthrust section of line 480, 45 km from the toe of the wedge (figure 2). Values beneath the first 10 km of the wedge lie in the range 0.55–0.70. These values are much less than predicted by models such those of Davis *et al.* (1983) which give $\lambda = 0.92$, but in these models λ at the decollement was assumed to be the same as λ in the wedge, for lack of information on what the variation in λ might be. In the frontal part of the wedge fluid pressure appears to be hydrostatic with λ varying between 0.62 near the seabed, and 0.49, just above the decollement. Lower fluid pressures in the wedge strengthen it and increase the shear stresses required at the base to give the wedge its taper, consequently lessening the degree of overpressuring required at the base. Even so, the values of λ are still too low to satisfy the model. A narrow zone of high porefluid pressures would, however, satisfy the tectonic constraints, but would not show up clearly in the type of velocity data used here. In the section of Line 465, where the sediments are predominantly clays, values of λ in excess of 0.85 are predicted in the region of the decollement 12–25 km from the toe of the wedge (figure 4).

Values of fluid pressure are likely to be underestimated by this method and so should be viewed with caution, because the assumption that the reference velocity/depth function derived from velocity data from the western Atlantic and the Barbados Ridge region (Bangs *et al.* 1990; Houtz 1981) represents a section in which pressures are hydrostatic may not be true. Any overpressuring in the regions from which the reference data were derived, will mean that the effective stresses derived from the reference function on the basis that they are hydrostatic will be overestimates. Also, uplift and compaction induced by tectonic stress will produce rocks that are overcompacted in relation to fluid pressures within them, according to the simple method of derivation of effective stress used here, and so erroneously low fluid pressures will be predicted. (The seismic velocity of a sample of rock from 1 km depth will not return to the value that it had shortly after deposition at the seabed when brought to the seabed.) Tectonic stress will increase the mean stress over that predicted from thickness of overburden. The Mohr–Coulomb model of the wedge of Davis *et al.* (1983) requires it to be at failure throughout, so the ratio the maximum to minimum principal effective stresses can be calculated from $(1+\sin\phi)/(1-\sin\phi)$ where ϕ is the angle of friction (Dahlen 1984). This ratio would typically be about 3. If λ is 0.6 then the effective stress is 40% of the total mean stress, and so the ratio of maximum to minimum principal stress would be 1.5. In the absence of tectonic stresses it is common to assume that all stresses are equal to the lithostatic load. In the presence of tectonic stresses, the lithostatic load will be an underestimate of the mean stress and this alone will lead to an underestimate of fluid pressure. Taking the limiting case of the lithostatic load being the minimum principal stress, if a value of $\lambda = 0.6$ is calculated from this rather than the mean stress, then the true value of $\lambda = 0.67$.

The zones of high fluid pressure correspond (as they must do given their manner of derivation) to regions of undercompaction. The greatest undercompaction occurs in the region of the decollement and just beneath it on this and the other two seismic lines north and south of it (Bangs *et al.* 1990). This is not surprising, because the

PHILOSOPHICAL TRANSACTIONS OF THE ROYAL SOCIETY A MATHEMATICAL, PHYSICAL & ENGINEERING SCIENCES

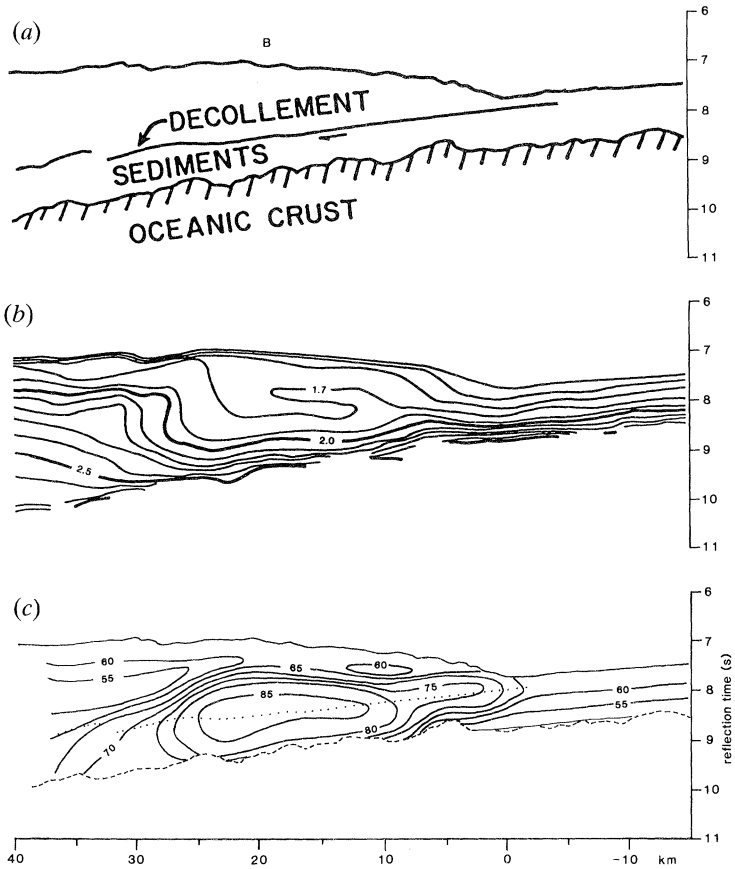

Figure 4. Relationship between fluid pressure inferred from seismic velocity and structure at the front of the Barbados Ridge Complex, seismic line 465, 16° 12′ N. The legend is as for figure 2. The sediments at 16° 12′ N are predominantly clays, whereas the upper 1.9 km of sediments at 14° 22′ N are the distal part of a submarine fan, incorporating silts and possibly sands.

sediments are among the least permeable in the section, and undergo the greatest rate of increase in load. Moore *et al.* (1990) report a similar situation in the accretionary wedge of the Nankai Trough off Japan, from preliminary results of seismic experiments. There, the underthrust pelagic section beneath the decollement shows little or no velocity increase with depth, and there is a downward velocity decrease across the decollement, contrasting with a downward velocity increase across the same stratigraphic level in the sediments beneath the trench.

3. Amplitudes of seismic reflectors

The amplitudes of reflections can be used to derive the changes in acoustic impedance (product of velocity and density) across boundaries. If these are boundaries of zones such as faults or decollements that act as fluid conduits, then the difference in fluid pressure may be inferred from the change in acoustic impedance. Cloos (1984) suggested that the seismic visibility of landward dipping reflectors in many accretionary wedges was a consequence of their activity as fluid conduits. Aoki

et al. (1985) inverted a seismic-reflection section across the Nankai Trough, using well log data from Deep Sea Drilling Project (DSDP) site 583F as a control, to obtain an acoustic impedance section. This showed a reduction in acoustic impedance beneath the decollement at the base of the toe of the accretionary wedge and zones of low impedance along thrusts cutting through the wedge. These zones of low impedance could be produced by a relatively high porosity associated with fluid overpressuring.

The decollement reflector beneath the Barbados Ridge accretionary wedge at 16° 12′ N (figure 4) shows a progressive change in amplitude and character as it extends westward beneath the wedge. At 20 km landward from the toe of the wedge, modelling of the seismic reflection section (Bangs & Westbrook 1991) indicates that the reflector is a 20 m thick layer of lower acoustic impedance than the rocks above and below (figure 5). At Ocean Drilling Project (ODP) site 671 where the decollement zone was penetrated it was found to be a zone of sheared clays 40 m thick (Moore *et al.* 1988). The porosity of the clay in the decollement zone was similar to (in fact, slightly less than) the porosities of clays immediately above and below it (Taylor & Leonard 1990). The proposed explanation for the seismic reflector is that the inner 20 m of the decollement zone has raised pore fluid pressure with consequently reduced effective stress and greater porosity, relative to the sediments above and below. The necessary reduction in acoustic impedance is given by a reduction of seismic velocity from 1.95 to 1.75 km s^{-1} with a concomitant reduction in density from 2023 to 1796 kg m^{-3}, an increase in porosity from 0.41 to 0.55. This implies a volume increase, under the effects of increased fluid pressure, of 30% of original volume.

The range of published values for the compressibility of clay, 10^{-6}–10^{-8} Pa^{-1} (Freeze & Cherry 1979) and the value used by Shi & Wang (1988) in modelling fluid pressures, indicate that a probable value for the clay in the decollement zone would be 10^{-7} Pa^{-1}. If so, an increase in fluid pressure of 2.6 MPa is required to inflate the decollement zone. An effective stress of 3.1 MPa, and lithostatic load of 23.1 MPa in the sediment directly overlying the decollement were estimated in the same manner as for Line 480 giving a value for λ of 0.87. Consequently, in the decollement zone the increased fluid pressure reduces effective stress to 0.5 MPa and raises λ to 0.98. Consolidation tests on core samples from the Barbados accretionary wedge (Taylor & Leonard 1990) show that if the initial effective stress were 3.1 MPa, a reduction to about 0.05 MPa would be needed to give the required change in porosity, implying fluid pressure very close to lithostatic, with $\lambda = 0.998$. At high fluid pressure (low effective mean stress), the effect of deviatoric stresses in producing dilation can be significant, and so the values of fluid pressure derived from simple elastic relaxation as above, are likely to be in error. Even so, the data indicate the value of λ for the decollement zone is above 0.95.

There are lateral variations over several hundred metres in the amplitude of the decollement reflector which have been shown by Bangs & Westbrook (1991) to be caused by changes in the acoustic impedance rather than changes in the thickness of the decollement layer. If this is correct, and the amplitude variation is not produced by some three-dimensional effect not accounted for in the two-dimensional model, then lateral changes in fluid pressure could be the cause of these changes in amplitude. The lateral variations in velocity of 1.75–1.88 km s^{-1} requires a volume change of 20% of original volume, which would imply a change in pressure of 1.8 MPa if compressibility is 10^{-7} Pa. Using the Leonard & Taylor data, a reduction

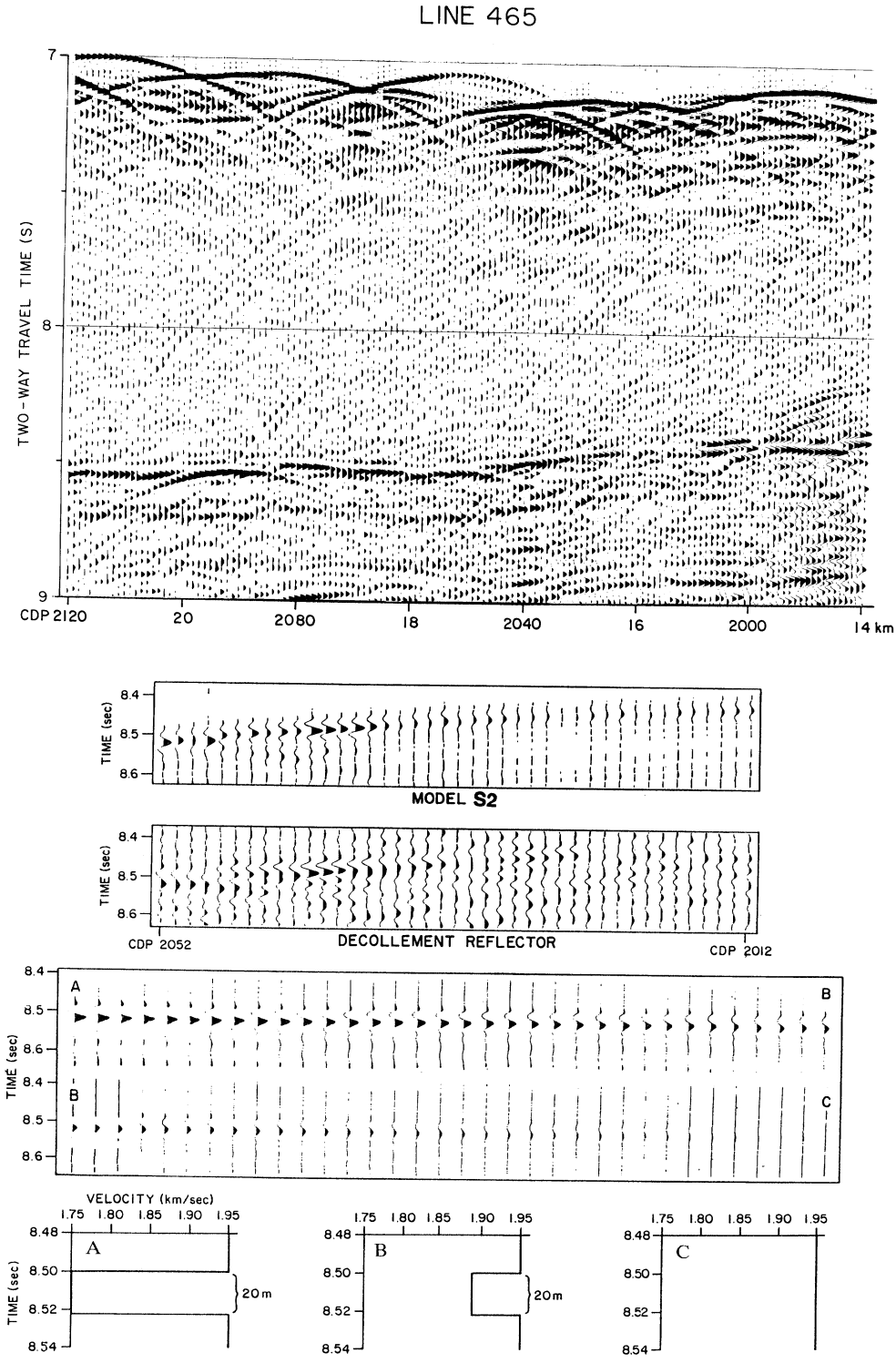

Figure 5. For description see opposite.

in pressure of about 2 MPa is indicated. This pressure change occurs over about 500 m, giving a horizontal pressure gradient of 4000 Pa m^{-1}. Leonard & Taylor measured a permeability of 6.48×10^{-21} m^2 (for viscosity of water of 10^{-3} Pa s) for a claystone close to but not from the decollement. If this value were representative of the decollement, the inferred pressure gradient would drive fluid at a Darcian velocity of 2.6×10^{-14} m s^{-1}, or 5.2×10^{-14} m s^{-1} average linear velocity (the rock has 0.5 porosity). The rate of subduction is 6.3×10^{-10} m s^{-1}, so with this low permeability the decollement could never transmit fluid to the toe of the wedge, but that has been shown to happen by the geochemistry of pore water in the ODP Leg 110 area. Screaton *et al.* (1990) on similar grounds assign a permeability of 10^{-14} m^{-2} to the decollement layer in their models. This higher permeability would yield any average flow rate of 8×10^{-8} m s^{-1} (2.5 m a^{-1}). Fisher & Hounslow (1990) estimate flow rates of 6.2 m a^{-1} along the decollement from variations in fluid temperature along the decollement measured in ODP Leg 110. If the value of 6.48×10^{-21} m^2 is representative of the intrinsic permeability of clay in the decollement layer then the bulk permeability of the layer must be controlled by the fracture permeability of the many shear surfaces developed parallel to the layer.

4. Heat flow

The advection of heat by water flowing out of the seabed produces an upwardly convex geothermal gradient than can be detected by heat flow probe measurements if the rate of flow (Darcian velocity) exceeds about 3×10^{-9} m s^{-1} (0.1 m a^{-1}) (Langseth & Herman 1981). The rates of diffuse outflow of water from wedges produced by compaction, predicted by a variety of models, do not exceed 3×10^{-10} m s^{-1} (0.01 m a^{-1}) (Minshull & White 1989; Langseth *et al.* 1990; Screaton *et al.* 1990; Le Pichon *et al.* 1990). Consequently, measurements of heat flow at the seabed do not offer a means of determining the 'background' rate of dewatering of accretionary wedges. The focused outflow of water through faults and other features can be detected by heat-flow measurements. If flow rates exceed 0.1 m a^{-1} they can be detected from the curvature of the thermal gradient, but more commonly it is the effect upon surface heat flow of introducing heat into the subsurface structure that is seen. Warm water flowing up a thrust fault will increase heat flow in the overlying thrust slice with the increase being greatest at the tip of the thrust slice. This gives the opposite heat-flow pattern to that produced by thrusting alone upon the conductive thermal régime, which is to reduce heat flow at the tip of the thrust slice because it is moving over the cool near-surface sediments. These effects have been modelled by Shi *et al.* (1988) off Oregon, and by Henry *et al.* (1989) for local heat-flow variations around seeps in the Nankai Trough.

An example of the relationship of the variation of heat flow in relation to thrusting comes from the southern Barbados Ridge complex at 12° 18′ N (figure 6). Heat-flow data from Foucher *et al.* (1990) and unpublished results from cruise 2907 of the

Figure 5. Part of seismic section 465 from the Barbados Ridge accretionary complex (see B on figure 4), with detail of the decollement reflector which can be modelled as a layer of low acoustic impedance 20 m thick (Bangs & Westbrook 1991). Variations in the amplitude of the reflector are best modelled by varying the acoustic impedance of the layer rather than its thickness. This variation is illustrated through models A, B, C. The model section, S2, is compared with the real section in the two central panels.

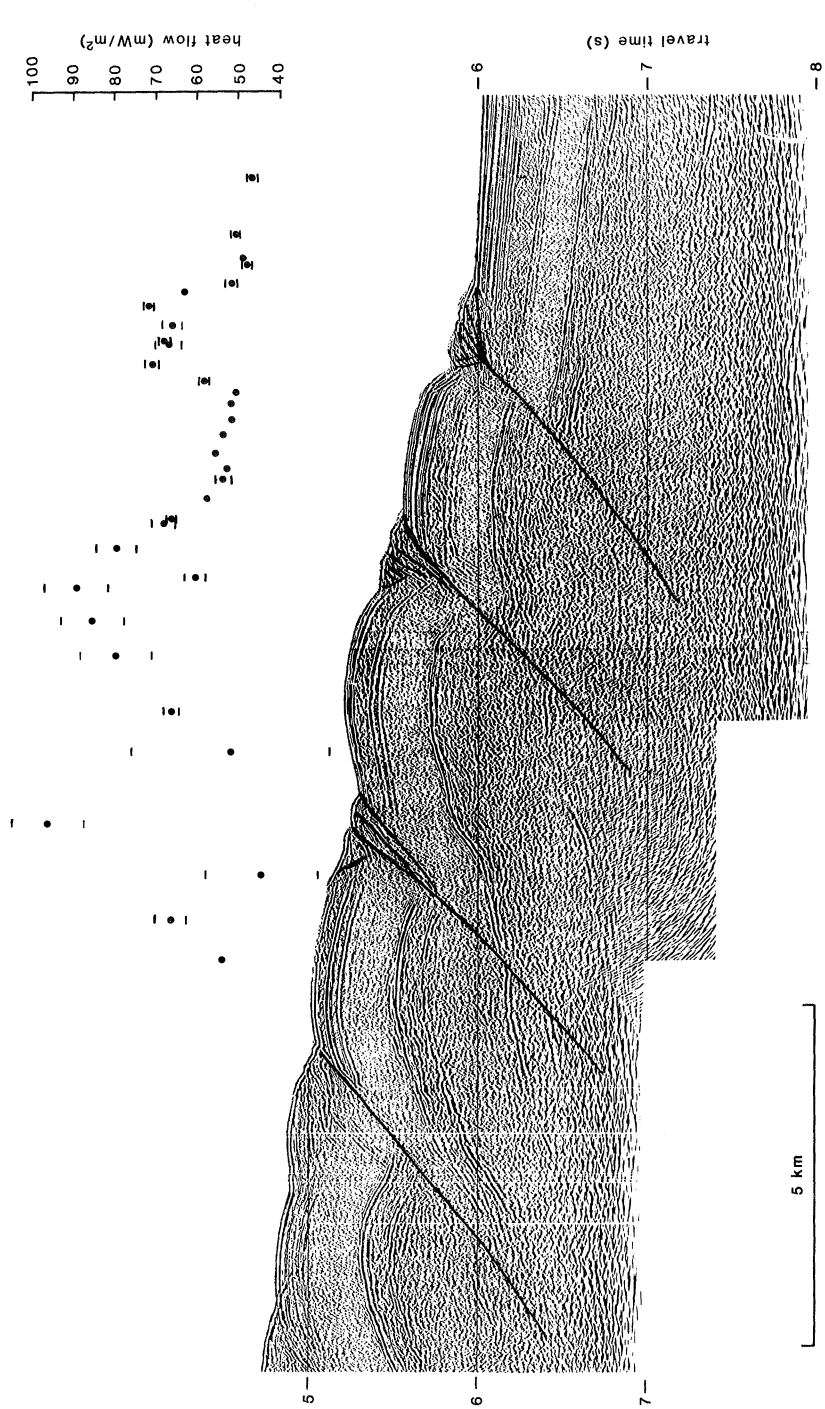

Figure 6. Heat flow across the toe of the Barbados Ridge accretionary complex at 12° 18′ N measured along a high resolution seismic profile (Westbrook *et al.* 1984). Heat flow from the thrust-outcrop wedge at the toe of the wedge is raised by 40 % relative to the ocean floor before it. This is attributed to warm fluids flowing up the thrust. Raised heat flow at the tip of the second thrust slice is more broadly distributed as a consequence of the longer period of warming. Error bars indicate standard deviations of heat flow measurements greater than 1 mW m^{-2}.

Robert D. Conrad show raised values of heat flow in the regions of the outcrops of the thrusts. For the frontal thrust all the high values come from the thrust-outcrop wedge. They are about 40% higher than those from the section in front of the accretionary wedge. The measured thermal gradients are not noticeably nonlinear. The higher heat flow at this thrust-outcrop wedge has been explained by warm fluids migrating up the thrust fault and through several small thrusts within the thrust-outcrop wedge (Foucher *et al.* 1990). Heat flow from the first anticline returns to nearly the same value as from the ocean floor, and rises again over the second thrust-outcrop wedge. Heat flow does not, however, decrease so quickly over the second anticline. This rise in heat flow over the forward part of the anticline is probably caused by the conductive diffusion of heat from warm water flowing along the second thrust, or it may be produced directly by upward flow of the warm water. In either case, time is required for the effect to be seen at the surface, which is why it is shown in the second anticline rather than the first, which it predates in age of formation by about 100000 years (the characteristic time for thermal diffusion from a source at 1 km depth is about 75000 years). The average increase in heat flow from the second thrust-outcrop wedge and the second anticline is 20 mW m^{-2}. Over the total width of the two features of 4.5 km the total heat flow is 90 W (per metre of strikelength). The rate of flow of water along the thrust required to produce this is 11 m^3 a^{-1}, assuming that heat flow is steady state and that the water comes from the decollement at a depth of 2 km with an initial temperature of 60 °C and cools to the temperature of seawater by the time it flows out from the seabed. This value, which is an underestimate of the flow, is between one third and one sixth of the volume of fluid in the pore space of sediment accreted to or underthrust beneath the accretionary wedge each year (Foucher *et al.* 1990). Measurement of temperatures by Fisher & Hounslow (1990) across thrusts intersected by drill holes in the northern part of the Barbados Ridge Complex, shows that fluids travel along the faults in pulses of limited duration (tens of years).

Heat-flow data for accretionary wedges are quite sparse. Measurements of heat flow in the seabed made with a thermistor probe are time consuming. If the seabed is hard it may be impossible to get the probe to penetrate it. The three regions where most direct measurements have been made are Barbados (Langseth *et al.* 1988; Langseth *et al.* 1990; Foucher *et al.* 1990), Nankai (Yamano *et al.* 1984; Kinoshita & Kasumi 1988), and Vancouver (Davis *et al.* 1990). Smaller numbers of measurements exist for southern Chile (Cande *et al.* 1987) and Washington-Oregon (Shi *et al.* 1988). Heat flow can be estimated from the depths of bottom simulating seismic reflectors (BSRs) which are common in accretionary wedges (Shipley *et al.* 1979). The reflector is produced at the base of a solid methane hydrate which is stable in the upper few hundred metres, where the temperature is low in relation to pressure, because of the depth of water. The rise of temperature with increasing depth makes the hydrate unstable. The BSR occurs along the phase boundary between solid hydrate and methane and water, and so is a measure of temperature at the depth of the BSR. The temperature dependence may be used to derive the thermal gradient and hence heat flow. Yamano *et al.* (1982) applied the approach to the Nankai Trough and it has been applied to a limited extent elsewhere (Cande *et al.* 1987; Minshull & White 1989; Davis *et al.* 1990; Ferguson *et al.* 1991). Minshull & White (1989) used the shallowing of the BSR in the regions of thrust faults in the accretionary wedge of the Makran to infer the flow of warm pore fluids along the faults. Off Vancouver, Davis *et al.* (1990) found the temperature estimated for the BSR, by using the phase diagram for

methane hydrate and water, to be 7 °C less than that estimated from downward extrapolation of the thermal gradient at the seabed. This difference can be explained if there is significant advection of heat by upward fluid flow. Davis *et al.* estimated a rate of 8×10^{-10} m s^{-1} for this flow, which is very large, and inconsistent with outflow estimated from compaction models by an order of magnitude (E. Davis, personal communication). Uncertainties over the mode of formation of hydrate in nature, including pore-water chemistry, have probably reduced the extent to which people have been prepared to apply this approach with confidence. For example, if the methane in the Vancouver margin is thermogenic, which is quite possible given the high geothermal gradient, then propane could be present. Only 1% propane is required to raise the temperature for hydrate stability by 7 °C (Sloan 1990). The presence of a BSR may also be taken as an indicator of fluid flow, if fluid flow is required to transport sufficient methane into the near-surface sediments to form a hydrate, rather than those sediments being sufficiently rich in organic carbon to generate the hydrate *in situ*. The degree to which flow is required to generate a BSR is an unresolved issue. Also, the formation of a hydrate will, to a varying extent, reduce the permeability of the sediment within which it is formed by filling pore spaces.

5. Summary

Seismic data have been of great value in providing images of the subsurface structure of accretionary wedges to identify possible fluid pathways, the state of compaction of sediments, the structural mechanisms by which compaction may be produced, and limiting estimates of fluid pressures. In the future, alongside continued progress in imaging, will be a greater and more detailed employment of velocity, amplitude and attenuation information to derive the influence of fluid on the behaviour of sediments in accretionary wedges from its effect on their physical properties. Although difficult to use in the submarine settings of accretionary wedges, this future work should make use of S-waves to better constrain changes in fluid content and to detect the alignment of the structural fabric which guides fluid flow.

Heat-flow data can be used directly or indirectly to derive rates of fluid flow. They are limited by the difficulty of obtaining measurements rapidly, but they can provide powerful constraints upon models, especially when three-dimensional information is obtained through boreholes. Gas hydrate BSRs, potentially provide a powerful approach for examining heat-flow variation over wide areas, if uncertainties over their mode of formation can be adequately resolved.

References

Aoki, Y., Kinoshita, H. & Kagami, H. 1985 Evidence of a low-velocity layer beneath the accretionary prism of the Nankai Trough: inferences from a synthetic sonic log. *Initial Rep. DSDP* **87**, 727–735.

Bangs, N. L. B., Westbrook, G. K., Ladd, J. W. & Buhl, P. 1990 Seismic velocities from the Barbados Ridge Complex: indicators of high pore-fluid pressures in an accretionary complex. *J. geophys. Res.* **95**, 8767–8782.

Bangs, N. L. B. & Westbrook, G. K. 1991 Seismic modelling of the decollement zone at the base of the Barbados Ridge accretionary complex. *J. geophys. Res.* (In the press.)

Bray, C. J. & Karig, D. E. 1985 Porosity of sediments in accretionary prisms and some implications for dewatering processes. *J. geophys. Res.* **90**, 768–778.

Cande, S. C., Leslie, R. B., Parra, J. C. & Hobart, M. 1987 Interaction between the Chile Ridge and the Chile Trench: geophysical and geothermal evidence. *J. geophys. Res.* **92**, 495–520.

Cloos, M. 1984 Landward-dipping reflectors in accretionary wedges: active dewatering conducts? *Geology* **12**, 519–522.

Dahlen, F. A. 1984 Noncohesive critical Coulomb wedges: an exact solution. *J. geophys. Res.* **89**, 10125–10133.

Davis, D. M., Suppe, J. & Dahlen, F. A. 1983 Mechanics of fold-and-thrust belts and accretionary wedges. *J. geophys. Res.* **88**, 1153–1172.

Davis, E. E., Hyndman, R. D. & Villinger, H. 1990 Rates of fluid expulsion across the northern Cascadia accretionary prism: constraints from new heat flow and multichannel seismic reflection data. *J. geophys. Res.* **95**, 8869–8889.

Ferguson, I. J., Westbrook, G. K., Langseth, M. G. & Thomas, G. P. 1991 Heat flow from the Barbados Ridge accretionary complex: comparison with conductive models. *J. geophys. Res.* (In the press.)

Fisher, A. T. & Hounslow, M. W. 1990 Transient fluid flow through the toe of the Barbados accretionary complex: constraints from Ocean Drilling Program Leg 110 heat flow studies and simple models. *J. geophys. Res.* **95**, 8845–8858.

Foucher, J. P., Le Pichon, X., Lallemant, S., Hobart, M. A., Henry, P., Benedetti, M., Westbrook, G. K. & Langseth, M. G. 1990 Heat flow tectonics, and fluid circulation at the toe of the Barbados Ridge accretionary prism. *J. geophys. Res.* **95**, 8859–8867.

Fowler, S. R., White, R. S., & Louden, K. E. 1985 Sediment dewatering in the Makran accretionary prism. *Earth planet. Sci. Lett.* **75**, 427–438.

Freeze, R. A. & Cherry, J. A. 1979 *Groundwater*. Englewood Cliffs, New Jersey: Prentice Hall.

Hamilton, L. 1978 Sound velocity-density in seafloor sediments and rocks. *J. acoust. Soc. Am.* **63**, 366–377.

Henry, P., Lallemant, S. J., Le Pichon, X. & Lallemand, S. F. 1989 Fluid venting along Japanese trenches: tectonic context and thermal modelling. *Tectonophysics* **160**, 277–291.

Houtz, R. E. 1981 Comparison of velocity-depth characteristics in western North Atlantic and Norwegian Sea sediments. *J. acoust. Soc. Am.* **68**, 1409–1414.

Kinoshita, M. & Kagumi, Y. 1988 Heat flow measurements in the Nankai Trough area. In *Preliminary Report of the Hakuko Maru Cruise KH 86-5* (ed. A. Taira), University of Tokyo Ocean Research Institute, 190–206.

Ladd, J. W., Westbrook, G. K., Buhl, P. & Bangs, N. 1990 Wide-aperture seismic profiles across the Barbados Ridge Complex. In *Proc. Ocean Drilling Program Initial Rep. b* **110**, 3–6.

Langseth, M. G. & Herman, B. M. 1981 Heat transfer in the oceanic crust of the Brazil Basin. *J. geophys. Res.* **86**, 10805–10819.

Langseth, M. G., Westbrook, G. K. & Hobart, M. A. 1988 Geophysical survey of a mud volcano seaward of the Barbados Ridge accretionary complex. *J. geophys. Res.* **93**, 1049–1061.

Langseth, M. G., Westbrook, G. K. & Hobart, M. A. 1990 Contrasting geothermal regimes of the Barbados Ridge accretionary complex. *J. geophys. Res.* **95**, 8829–8843.

Le Pichon, X., Henry, P. & Lallemant, S. 1990 Water-flow in the Barbados accretionary complex. *J. geophys. Res.* **95**, 8945–8967.

Moore, G. F., Shipley, T. H., Stoffa, P. L., Karig, D. E., Taira, A., Kuramoto, S., Tokugama, H. & Suyehiro, K. 1990 Structure of the Nankai Trough accretionary zone from multichannel seismic reflection data. *J. geophys. Res.* **95**, 8753–8765.

Moore, J. C., Mascle, A., Taylor, E. & Shipboard Party. 1988 Tectonics and hydrogeology of the northern Barbados Ridge: results from Ocean Drilling Program Leg 110. *Geol. Soc. Am. Bull.* **100**, 1578–1593.

Minshull, T. A. & White, R. S. 1989 Sediment compaction and fluid migration in the Makran accretionary prism. *J. geophys. Res.* **94**, 7387–7402.

Screaton, E. J., Wuthrich, D. R. & Dreiss, S. J. 1990 Permeabilities, fluid pressures, and flow rates in the Barbados Ridge Complex. *J. geophys. Res.* **95**, 8997–9007.

Shi, Y. & Wang, C. Y. 1988 Generation of high pore pressures in accretionary prisms: inferences from the Barbados subduction complex. *J. geophys. Res.* **93**, 8839–8910.

PHILOSOPHICAL TRANSACTIONS OF THE ROYAL SOCIETY A MATHEMATICAL, PHYSICAL & ENGINEERING SCIENCES

Shi, Y., Wang, C. Y., Langseth, M. G., Hobart, M. A. & von Huene, R. 1988 Heat flow and thermal structures of the Washington–Oregon accretionary prism – a study of the lower slope. *Geophys. Res. Lett.* **15**, 1113–1116.

Shipley, T. H., Houston, M. H., Buffler, R. T., Shaub, F. J., McMillen, K. J., Ladd, J. W. & Worzel, J. L. 1979 Seismic evidence for widespread possible gas hydrate horizons on continental slopes and rises. *Am. Ass. Petrol. Geol. Bull.* **63**, 2204–2213.

Shipley, T. H. & Moore, G. F. 1986 Sediment accretion, subduction and dewatering at the base of the trench slope off Costa Rica: a seismic reflection view of the decollement. *J. geophys. Res.* **91**, 2019–2028.

Shipley, T. H., Stoffa, P. L. & Dean, D. F. 1990 Underthrust sediments, fluid migration paths, and mud volcanoes associated with the accretionary wedge of Costa Rica: Middle America Trench. *J. geophys. Res.* **95**, 8743–8752.

Sloan, E. D. 1990 *Clathrate hydrates of natural gases*. New York: Marcel Dekker.

Taylor, E. & Leonard, J. 1990 Sediment consolidation and permeability at the Barbados forearc. In *Proc. ODP Sci. Results* (ed. J. C. Moore *et al.*) 110: College Station, TX (Ocean Drilling Program), pp. 289–308.

Westbrook, G. K. & Smith, M. J. 1983 Long decollements and mud volcanoes: evidence from the Barbados Ridge Complex for the role of high pore-fluid pressure in the development of an accretionary complex. *Geology* **11**, 279–285.

Westbrook, G. K., Ladd, J. W., Buhl, P., Bangs, N. & Tiley, G. 1988 Cross section of an accretionary wedge: Barbados Ridge Complex. *Geology* **76**, 631–635.

Westbrook, G. K., Mascle, A. & Biju-Duval, B. 1984 Geophysics and structure of the Lesser Antilles forearc. *Initial Rep. DSDP* A**78**, 24–38.

Westbrook, G. K., Boulegue, J., Bowers, T. S., Cathles, L. M., Davis, E. E., Kastner, M., Langseth, M., Leinen, M. & Ohta, S. 1987 Fluid Circulation in the Crust and the Global Geochemical Budget. In *Rep. 2nd Conf. Scientific Ocean Drilling* (*COSODII*). European Science Foundation, Strasbourg, pp. 67–86.

Yamano, M. S., Honda, S. & Uyeda, S. 1984 Nankai Trough: a hot trench. *Mar. Geophys. Res.* **6**, 187–203.

Yamano, M. S., Uyeda, S., Aoki, Y. & Shipley, T. H. 1982 Estimates of heat flow derived from gas hydrates. *Geology* **10**, 339–343.

PHILOSOPHICAL TRANSACTIONS OF THE ROYAL SOCIETY A MATHEMATICAL, PHYSICAL & ENGINEERING SCIENCES